

# Optimal Preview Control Method of Multi-Objective Comprehensive Dynamics for Virtual Track Train Path Following

Rang Zhang\* and Gang Shen \*\*

**Keywords :** virtual track train, optimal preview control, path following, dynamic performance.

## ABSTRACT

This paper proposed an optimal preview control method of multi-objective comprehensive dynamics to improve the mobility of virtual track train (VTT) in the process of path tracking. A 6-DOF linear reference dynamic model of VTT is established, taking lateral speed, yaw rate, first articulation angle and second articulation angle as control variables, the train reference state variables are derived according to the known reference path information. Then, based on the optimal preview control theory and considering the constraints of VTT dynamics, a multi-objective comprehensive dynamic control algorithm is designed. Finally, to comprehensively analyze the feasibility of the algorithm, the robustness of the control algorithm to road adhesion conditions, speed and combined curve is verified respectively through the co-simulation of multi-body dynamics software and MATLAB/Simulink.

## INTRODUCTION

In recent years, a new urban traffic mode has emerged in small and medium-sized cities in China, called virtual rail train (VTT), as shown in Fig. 1. The system mainly includes advanced assistant driving of front car body, active tracking function of rear car bodies, lane line and pedestrian identification technology, active steering mechanism, high-performance body design, hydraulic articulated device, adaptive suspension, etc. The VTT can be used as a

solution to congestion in medium-sized cities or as a supplement to transportation in large cities, which is in line with China's basic national conditions and public transport development strategy. (Han et al., 2015)

This technology is also used in the public transportation system of other countries and has realized engineering. The German Siemens CIVIS IRISBUS public transport system (Georges.,2012) the French TEOR public transport system (Boucheret.,2004) and the German AUTOTram public transport system (Wagner et al., 2013) all adopt the optical recognition guidance technology. Phileas public transport system of VDL group in the Netherlands adopts track nail guidance technology. The 'Intelligent rail express system' developed by Zhuzhou Research Institute of CRRC in China adopts self-developed "Virtual track following control". (Yuan et al., 2020)

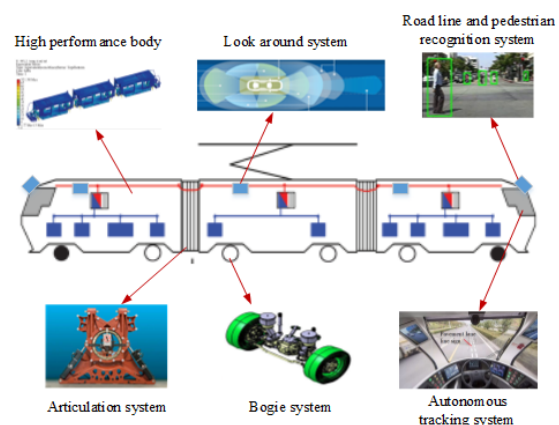


Fig. 1. VTT system.

There are some literatures on the control methods of rubber-wheel articulated train. Sampei et al. (1995) established the nonlinear kinematics model of articulated vehicle, and designed a path tracking controller for articulated vehicles (semi-trailer vehicle) by using time scale transformation and accurate linearization. However, the control method under variable curvature path is not studied in the paper. Bolzern et al. (2001) used input-output feedback

*Paper Received January, 2023. Revised July, 2023. Accepted August, 2023. Author for Correspondence: Rang Zhang.*

\* PhD student, Rail Transit Institute, Tongji University, Shanghai 201804, China.

\*\* Professor, Rail Transit Institute, Tongji University, Shanghai 201804, China.

linearization to realize the steering control of multi articulated vehicles. Similarly, the controller in this literature is stable in a circular curve with constant radius of curvature, and has not been studied under complex road conditions. Astolfi et al. (2004) used the Lyapunov function method to track the straight-line and circular arc routes of multi articulated vehicle trains. Yamaguchi et al. (2014) proposed a path tracking feedback algorithm for five axle three steering coupled vehicle system by using linear control theory and Lyapunov's second method. The above literatures are studied from the perspective of kinematics, and the dynamic characteristics of the train cannot be obtained, especially the stability and tire wear of the train when turning at medium and high speed on the small radius curve.

Most of the above studies use classical control theory, especially PID control, which considers less state information, and often cannot take into account other performance of the train, such as the problem of too large centroid sideslip angle of the car body.

Motivated by the above issues, the main contributions of this paper are as follows:

- (1) According to the known reference path information, the linear reference dynamic model of the VTT is established to form a reference variable sequence including dynamic indexes, taking into account the path following performance and yaw stability.
- (2) By constructing train dynamic constraints, the train can adapt to different road adhesion conditions, different speeds and the continuous change of curvature radius of combined path when following the reference path.
- (3) The preview desired values information is used as the inherent characteristics of the system, the objective function is constructed, and the path following performance and stability requirements are considered to realize the optimal following of the VTT to the reference path.

### STRUCTURE OF THE VTT

The VTT is a two-way multi marshalling rubber-tired train with 100% low floor frame, all electric drive and multiple power receiving modes (Feng et al. 2020). Fig. 2(a) shows the formation mode of VTT. The whole train adopts the form of three modules and six axles. There is a bogie at the front and rear of each car, of which the front and rear car bodies are powered bogies, the other are non-power bogies, and the car bodies are connected by the articulated disc. The power bogie includes rubber wheels, air suspension, deceleration device and brake actuator, as shown in Fig. 2(b). And the non-power bogie includes rubber wheel, air suspension, brake actuator and central spring energy storage parking brake (as safety braking device), as shown in Fig. 2(c).

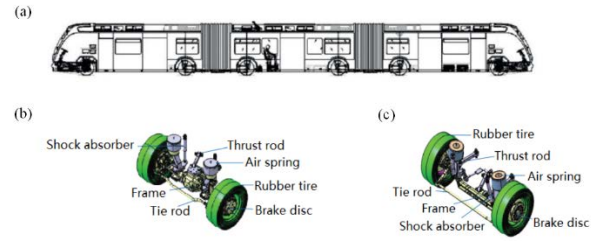


Fig. 2. Structure of VTT: (a) train formation mode, (b) power bogie, (c) non-power bogie.

## VTT REFERENCE DYNAMICS

### MODEL

In order to simulate the lateral dynamic characteristics of the VTT, a linear model of train dynamics is established. XOY is the geodetic coordinate system, and the local coordinate system  $x_i, y_i$  for each car body are established. The coordinate origin of each car body coordinate system is located at the center of mass. The direction along the longitudinal axis of the car body is the x axis, and the direction perpendicular to the longitudinal axis is the y axis. Ignoring the influence of suspension system, the vertical and roll motion of the train are not considered, and ignoring the influence of aerodynamics, the air resistance is not considered. The lateral dynamics model of the train with 6 degrees of freedom is established, including the lateral and yaw motions of three car bodies as shown in Fig. 3.  $F_{y1fl}, F_{y1fl}, F_{y1fl}, F_{y1fl}$  are the lateral forces of each tire on the front car body, respectively.  $F_{y2fl}, F_{y2fl}, F_{y2fl}, F_{y2fl}$  are the lateral forces of each tire on the middle car body, respectively.  $F_{y3fl}, F_{y3fl}, F_{y3fl}, F_{y3fl}$  are the lateral forces of each tire on the rear car body, respectively.

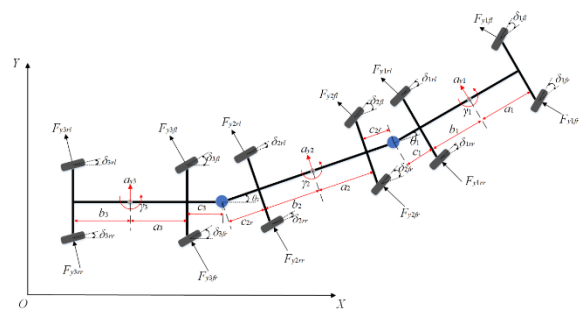


Fig. 3. Overall force analysis of the train.

Lateral dynamic equations of VTT are written in matrix form as matrix form are obtained  $P\dot{X} + QX = RU$ . The corresponding state space expression can be written, see the Appendix for element expressions in each matrix.

$$\begin{cases} \dot{X} = AX + BU \\ Y = CX \end{cases} \quad (1)$$

Where  $X = [\beta_1 \ \gamma_1 \ \theta_1 \ \dot{\theta}_1 \ \theta_2 \ \dot{\theta}_2]$ ,  $A = P^{-1}Q$ ,  $B = P^{-1}R$ .

$$C = \begin{bmatrix} 0 & 0 & 0 & 0 & 0 & 0 \\ 0 & 1 & 0 & 0 & 0 & 0 \\ 0 & 0 & 1 & 0 & 0 & 0 \\ 0 & 0 & 0 & 0 & 0 & 0 \\ 0 & 0 & 0 & 0 & 1 & 0 \\ 0 & 0 & 0 & 0 & 0 & 0 \end{bmatrix},$$

$$U = [\delta_{1fl} \delta_{1fr} \delta_{1rl} \delta_{1rr} \delta_{2fl} \delta_{2fr} \delta_{2rl} \delta_{2rr} \delta_{3fl} \delta_{3fr} \delta_{3rl} \delta_{3rr}],$$

$$P = \begin{bmatrix} p_{11} & p_{12} & p_{13} & p_{14} & p_{15} & p_{16} \\ p_{21} & p_{22} & p_{23} & p_{24} & p_{25} & p_{26} \\ p_{31} & p_{32} & p_{33} & p_{34} & p_{35} & p_{36} \\ p_{41} & p_{42} & p_{43} & p_{44} & p_{45} & p_{46} \\ 0 & 0 & 0 & 1 & 0 & 0 \\ 0 & 0 & 0 & 0 & 0 & 1 \end{bmatrix},$$

$$Q = \begin{bmatrix} q_{11} & q_{12} & q_{13} & q_{14} & q_{15} & q_{16} \\ q_{21} & q_{22} & q_{23} & q_{24} & q_{25} & q_{26} \\ q_{31} & q_{32} & q_{33} & q_{34} & q_{35} & q_{36} \\ q_{41} & q_{42} & q_{43} & q_{44} & q_{45} & q_{46} \\ 0 & 0 & 0 & 1 & 0 & 0 \\ 0 & 0 & 0 & 0 & 0 & 1 \end{bmatrix}$$

$$R = \begin{bmatrix} r_{11} & r_{12} & r_{13} & r_{14} & r_{15} & r_{16} & r_{17} & r_{18} & r_{19} & r_{110} & r_{111} & r_{112} \\ r_{21} & r_{22} & r_{23} & r_{24} & r_{25} & r_{26} & r_{27} & r_{28} & r_{29} & r_{210} & r_{211} & r_{212} \\ 0 & 0 & 0 & 0 & r_{31} & r_{32} & r_{33} & r_{34} & r_{35} & r_{36} & r_{37} & r_{38} \\ 0 & 0 & 0 & 0 & 0 & 0 & 0 & 0 & r_{41} & r_{42} & r_{43} & r_{44} \\ 0 & 0 & 0 & 0 & 0 & 0 & 0 & 0 & 0 & 0 & 0 & 0 \\ 0 & 0 & 0 & 0 & 0 & 0 & 0 & 0 & 0 & 0 & 0 & 0 \end{bmatrix}$$

The lateral velocity of the front car body in the geodetic coordinate system can be obtained by using the speed, the centroid sideslip angle and the lateral yaw angular velocity of the front car body, as shown in Formula (2).

$$\dot{Y}_1 = v_x(\beta_1 + \gamma_1) \quad (2)$$

Adding Formula (2) to the train reference dynamics model, a new state equation combining the train state and lateral displacement is obtained, and the new status variable is  $X = [\beta_1 \gamma_1 \theta_1 \dot{\theta}_1 \theta_2 \dot{\theta}_2 \dot{Y}_1]$ .

The yaw rate can represent the stability of the vehicle, especially when the vehicle passes through the curve section. If the parameter equation of the reference path is shown in Formula (3).

$$\begin{cases} X = g(t) \\ Y = h(t) \end{cases} \quad (3)$$

Then the curvature of the reference path is

$$K = \frac{|g'(t)h''(t) - g''(t)h'(t)|}{[g'^2(t) + h'^2(t)]^{\frac{3}{2}}}$$

Thus, the desired value for yaw rate of the front car body can be obtained, as shown in Formula (4).

$$\gamma_{1d} = \frac{v_x}{R_{d1}} = v_x K \quad (4)$$

Fig. 4 shows the train status at two adjacent times after  $\Delta t$ ,  $(X_{it}, Y_{it})$  is the position coordinate of the car body centroid at time  $t$ ,  $(X_{i(t+\Delta t)}, Y_{i(t+\Delta t)})$  is

the position coordinate of the car body centroid at time  $(t + \Delta t)$ . When the centroid coordinate of the rear body at time  $t + \Delta t$  coincide with the centroid coordinate of the front body at time  $t$ , the desired articulation angle can be obtained.

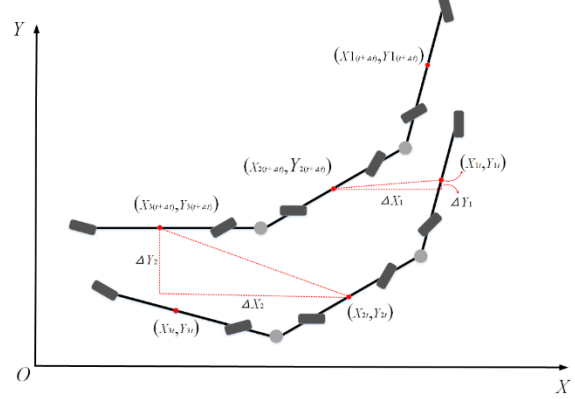


Fig. 4. Schematic diagram of trajectory following deviation of car bodies.

If the centroid position of the middle car body at  $t + \Delta t$  coincides with that of the front car body at  $t$ , then  $\Delta X_1 = 0$ ,  $\Delta Y_1 = 0$ .

Then

$$\tan(\varphi_{1d(t+\Delta t)} - \theta_{1d(t+\Delta t)}) = \frac{Y_{1(t+\Delta t)} - L_1 \sin \varphi_{1d(t+\Delta t)} - Y_{1t}}{X_{1(t+\Delta t)} - L_1 \cos \varphi_{1d(t+\Delta t)} - X_{1t}}$$

Therefore, the desired articulation angle between the front car body and the middle car body can be obtained.

$$\theta_{1d(t+\Delta t)} = \varphi_{1d(t+\Delta t)} - \arctan \left( \frac{Y_{1(t+\Delta t)} - L_1 \sin \varphi_{1d(t+\Delta t)} - Y_{1t}}{X_{1(t+\Delta t)} - L_1 \cos \varphi_{1d(t+\Delta t)} - X_{1t}} \right)$$

Where  $\varphi_{1dt} = \int_0^t \gamma_{1d}(t) dt$ ,  $\varphi_{1d(t+\Delta t)} = \int_0^{t+\Delta t} \gamma_{1d}(t) dt$ ,  $\Delta t = \frac{L_1 + L_2}{v_x}$ .

Similarly, the desired articulation angle between the rear car body and the middle car body can be obtained.

$$\theta_{2d(t+\Delta t)} = \varphi_{2d(t+\Delta t)} - \arctan \frac{Y_{2(t+\Delta t)} - L_1 \sin \varphi_{2d(t+\Delta t)} - Y_{2t}}{X_{2(t+\Delta t)} - L_1 \cos \varphi_{2d(t+\Delta t)} - X_{2t}}$$

Where  $\varphi_{2d(t+\Delta t)} = \int_0^{t+\Delta t} \gamma_{1d}(t) dt - \theta_{1d(t+\Delta t)}$ .

## DESIGN OF THE CONTROLLER

During the autonomous tracking of the front car body, the automatic tracking system extracts the lane line features and classifies them through the image recognition sensor, so as to form the discrete coordinate sequence of the reference digital track, as

shown in Fig. 5.

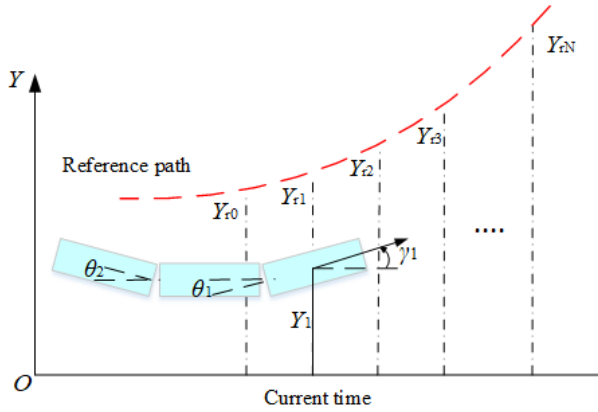


Fig. 5. Schematic diagram of trajectory following deviation of car bodies.

Firstly, the forward Euler method is used to discretize the combined state equation. The state program of the discrete-time system is shown in Formula (5).

$$\begin{cases} \dot{X}(k+1) = \tilde{A}X(k) + \tilde{B}u(k) \\ Y(k+1) = \tilde{C}X(k) \end{cases} \quad (5)$$

Where  $\tilde{A} = I + TA$ ,  $\tilde{B} = TB$ ,  $T$  is the sampling period.

Optimal preview control is to apply the idea of optimal control to find a control gain when the future information can be previewed, so that the quadratic objective evaluation function  $J$  including error term  $e(k)$  and control term  $u(k)$  takes the minimum value. (Murphy., 2004)

Define the error vector, as shown in Formula (6).

$$e(k) = R(k) - C(k)X(k) \quad (6)$$

According to Figure 6, the expression of each element in the error vector is derived, as shown in Formula (7).

$$\begin{cases} e_{Y_1}(k) = Y_r(k) - Y_1(k) \\ e_{vy_1}(k) \approx \frac{Y_r(k+1) - Y_r(k)}{T} - \dot{Y}_1 \\ e_{\gamma_1}(k) = \gamma_d \gamma(k) - \gamma(k) \\ e_{\theta_1}(k) = \theta_{1d}(k) - \theta_1(k) \\ e_{\theta_2}(k) = \theta_{2d}(k) - \theta_2(k) \end{cases} \quad (7)$$

In order to transform the following problem into the adjustment problem of the following error, the difference operator is introduced, and the first-order difference is taken for Formula (5) and Formula (6) to obtain Formula (8).

$$\begin{cases} \Delta X(k+1) = A\Delta X(k) + B\Delta u(k) \\ \Delta e(k+1) = \Delta R(k+1) + C\Delta u(k) \end{cases} \quad (8)$$

Set a new state variable according to Formula (35).

$$X_o(k) = \begin{bmatrix} e(k) \\ \Delta X(k) \end{bmatrix}$$

Thus, a new state space expression called tracking error system can be obtained, as follows.

$$\begin{bmatrix} e(k+1) \\ \Delta X(k+1) \end{bmatrix} = \begin{bmatrix} I & -CA \\ 0 & A \end{bmatrix} \begin{bmatrix} e(k) \\ \Delta X(k) \end{bmatrix} + \begin{bmatrix} CB \\ B \end{bmatrix} \Delta u(k) + \begin{bmatrix} 1 \\ 0 \end{bmatrix} \Delta R(k+1)$$

Further can be written as

$$\begin{cases} X_o(k+1) = WX_o(k) + G\Delta u(k) + G_R\Delta R(k+1) \\ \Delta Y(k) = C_o\Delta X_o(k) \end{cases}$$

Where  $W = \begin{bmatrix} I & -CA \\ 0 & A \end{bmatrix}$ ,  $G = \begin{bmatrix} CB \\ B \end{bmatrix}$ ,  $G_R = \begin{bmatrix} 1 \\ 0 \end{bmatrix}$ ,  $C_o = \begin{bmatrix} 0 & C \end{bmatrix}$

In order to make use of the known target values increment from the current time  $k$  to the future time  $k + M_r$  as the inherent characteristics of the system, the previewed state is defined, as follows.

$$X_R(k+1) = A_R X_R(k)$$

Where

$$X_R(k) = \begin{bmatrix} \Delta R(k+1) \\ \Delta R(k+2) \\ \vdots \\ \Delta R(k+M_r) \end{bmatrix}, A_R = \begin{bmatrix} 0 & I_m & \cdots & 0 \\ \vdots & \vdots & \ddots & \vdots \\ \vdots & \vdots & \cdots & I_m \\ 0 & \cdots & \cdots & 0 \end{bmatrix}$$

A new state variable is introduced to obtain the augmented system including the preview target values, as follows.

$$\begin{bmatrix} X_o(k+1) \\ X_R(k+1) \end{bmatrix} = \begin{bmatrix} W & G_p \\ 0 & A_R \end{bmatrix} \begin{bmatrix} X_o(k) \\ X_R(k) \end{bmatrix} + \begin{bmatrix} G \\ 0 \end{bmatrix} \Delta u(k)$$

Where  $G = \begin{bmatrix} 0 & G_R & 0 & \cdots & 0 \end{bmatrix}$ .

In order to realize the optimal adjustment of the system following error, the optimal evaluation function can be defined, as follows.

$$J = \sum_{k=1}^N \left\{ \begin{bmatrix} X_o^T(k) & X_R^T(k) \end{bmatrix} \begin{bmatrix} Q & 0 \\ 0 & 0 \end{bmatrix} \begin{bmatrix} X_o(k) \\ X_R(k) \end{bmatrix} + \Delta u^T(k) R \Delta u(k) \right\}$$

To ensure that the train does not lose stability in the process of running, when designing the optimal preview controller based on the train dynamics model, it is necessary to add VTT dynamics constraints. The constraints of centroid sideslip angle of each car body and road adhesion conditions are included in the paper.

The centroid sideslip angle of the car body has a great influence on the stability of the train, so the centroid sideslip angle must be limited to a reasonable range. The research in the literature (Van Zanten., 1998) shows that the limit of centroid sideslip angle of

the car body can reach  $\pm 12^\circ$  when the vehicle runs stably on the dry asphalt pavement with good adhesion. On the slippery road with low adhesion coefficient, the limit value is  $\pm 3^\circ$ . Therefore, this paper sets the constraint conditions of centroid sideslip angle as follows.

$$\begin{cases} -12^\circ < \beta_i < 12^\circ & (\text{High adhesion road}) \\ -3^\circ < \beta_i < 3^\circ & (\text{Low adhesion road}) \end{cases}$$

Where  $i = 1 \sim 3$ .

In addition, the train is also limited by the adhesion conditions between the tire and the ground, so it is necessary to add the constraints of tire/road adhesion conditions. The relationship between longitudinal acceleration and lateral acceleration limited by ground adhesion is as follows.

$$\sqrt{a_x^2 + a_y^2} \leq \mu g$$

In this paper, it is assumed that the train runs at a constant speed in the longitudinal direction, so it is further simplified.

$$-\mu g \leq a_{yi} \leq \mu g$$

Where  $i = 1 \sim 3$ .

Based on the above objective function and train dynamics constraints, the controller based on VTT dynamics model needs to solve the following optimization problems.

$$\begin{aligned} \min: J = & \sum_{k=1}^N \left\{ [X_o^T(k) \quad X_R^T(k)] \begin{bmatrix} Q & 0 \\ 0 & 0 \end{bmatrix} \begin{bmatrix} X_o(k) \\ X_R(k) \end{bmatrix} \right. \\ & \left. + \Delta u^T(k) R \Delta u(k) \right\} \\ \text{s.t.} & \begin{cases} -12^\circ < \beta_i < 12^\circ & (\text{High adhesion road}) \\ -3^\circ < \beta_i < 3^\circ & (\text{Low adhesion road}) \\ -\mu g \leq a_{yi} \leq \mu g \end{cases} \end{aligned}$$

Based on the above algorithm derivation, the forward preview program of VTT dynamics is compiled with MATLAB. The calculation steps are shown in Table 1. Set the sampling period  $T$  as 0.05s, the number of prediction steps  $Mr$  as 20, and  $N$  is the number of reference path points.

Table 1. Calculation flow of simulation program.

| Forward preview for train state target based on MATLAB  |
|---|
| <b>Step 1 Initialize</b> system state variables $X_0$ and control variables $U_0$                       |
| <b>Step 2 Set</b> sampling period $T$ and Simulation time $T_{all}$ .                                   |
| <b>Step 3 Input</b> reference path points $z_d=(zr_1, zr_2, zr_3 \dots zr_N)$ and set preview step $Mr$ |
| <b>Step 4 Discrete</b> the train linear reference model   |
| <b>Step 5 loop</b>  |
| $k=1: N$  |
| $j=1: Mr$   |

---

```

Generate the error vector
 $X_o(k)=[e(k) \quad \Delta X(k)]^T$ 
Generate preview desired values  $R(k+j)$ 
Construction augmentation system  $ss(A_a,$ 
 $B_a, C_a, D_a)$ 
end
end
Step 6 Generate constraint region  $cons(\beta_i, a_{yi})$ 
Step 7 Generate the optimal evaluation function  $J$ 
Step 8 Call quadratic programming solver
Step 9 Output control variables  $U^*$ 

```

---

## SIMULATION RESULTS

In this section, the nonlinear dynamic model of VTT is established by using multi-body dynamics software UM to verify the effectiveness of the control algorithm. Through the 'Co-simulation Tool' provided by the multi-body dynamics software UM, the information interaction between the dynamic model of VTT and the control module written based on Matlab/Simulink is realized, and the multi-objective comprehensive dynamic optimal preview control simulation platform for VTT trajectory tracking is established, as shown in Fig. 6.

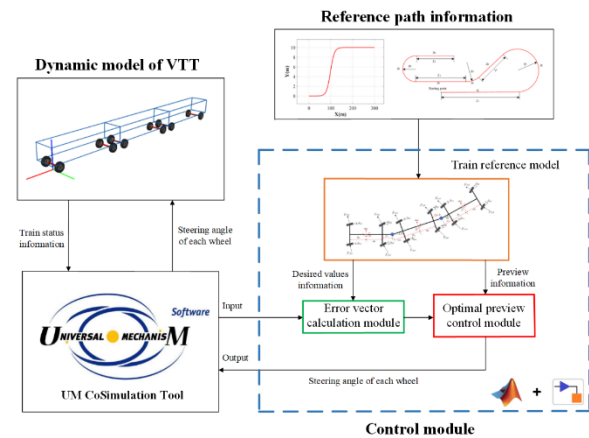


Fig. 6. Flow chart of co-simulation platform.

### Effectiveness of the Control Algorithm

To evaluate the effectiveness of the control algorithm and the stability of VTT in the path following process, a nonlinear lane changing route is selected as the reference path, and its parameter equation is shown he track diagram is shown in the Fig. 7.

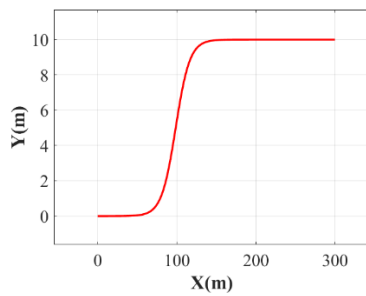


Fig. 7. Reference path trajectory.

Fig. 8 compares the control effect of adding preview information and not adding preview information in the process of the train following the reference path at 10m/s. It can be seen from Figure 8(a) that the control algorithm with preview information can ensure that the train has better adaptability to the continuous change of line curvature and higher response speed in the process of lane change. It can be seen from Fig. 8(c) that the maximum lateral deviation of the car body centroid is only 0.053m. It can be seen from Fig. 8(b) that the control algorithm without preview information has poor adaptability to the continuous change of line curve, slow response speed and obvious hysteresis, that is, the train does not have enough response time to the change of curve. It can be seen from Fig. 8(d) that the maximum lateral deviation of the car body centroid reaches 0.48m. In conclusion, the optimal preview control method of multi-objective comprehensive dynamics for VTT trajectory tracking is effective.

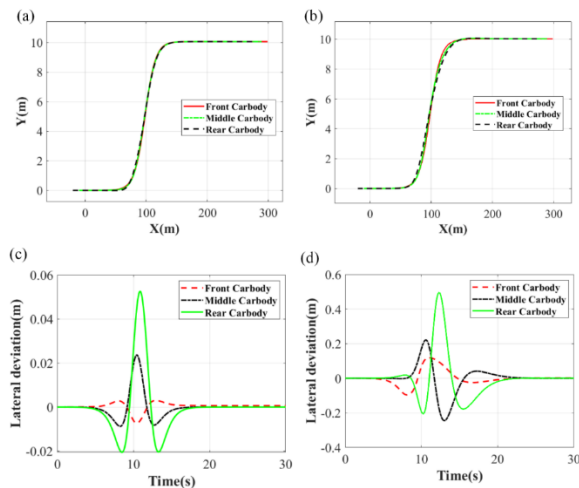


Fig. 8. Trajectory tracking control effect.

Fig. 9 is the variation curve of the dynamic performance index of VTT under the optimal preview control algorithm. It can also be seen from the Fig. 9(a) and Fig. 9(b) that the yaw rate of the front car body can follow the desired value quickly and stably, and the yaw rate of the middle and rear car bodies is basically synchronized with the trend and amplitude of the front car body, and the articulation angles of VTT can

accurately the desired values. It can be seen from Fig. 9(c) and Fig. 9(d) that the centroid sideslip angle and lateral acceleration of each car body of the train are in the stable range and far less than the critical value, indicating that the train has great stability.

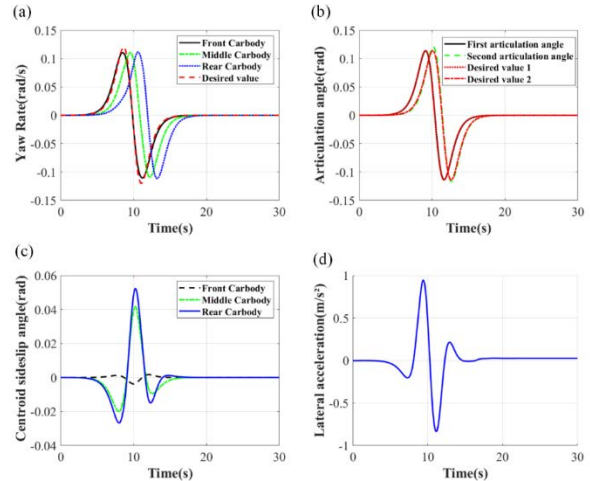


Fig. 9. Dynamic performance index with comprehensive optimal control algorithm.

### Analysis of Control Effect under Low Adhesion Pavement

When VTT runs on roads with different adhesion conditions, its dynamic performance parameters will change, mainly due to the change of tire cornering stiffness, resulting in insufficient lateral force provided by the ground, which brings some challenges to the performance of the controller. Therefore, it is necessary to verify the effectiveness of the control algorithm on the low adhesion road. In this paper, the wet and slippery pavement with the adhesion coefficient  $\mu=0.4$  is used for calculation and analysis, and the simulation results are shown in Fig. 10.

Fig. 10 (a) shows that the train can still follow the reference path on the low adhesion road at 10m/s. Fig. 10(b) and Fig. 10(c) also show that the yaw rate of each car body and the articulation angle between car bodies can quickly follow the desired value and remain stable. On the low adhesion road, because the ground cannot provide sufficient lateral force, the train will cause large lateral deviation during lane change, and the controller can correct the deviation in time. As shown in Fig. 10(d), the maximum deviation is 0.092m and finally converges to 0.

Fig. 10(e) and Fig. 10(f) show that the centroid sideslip angle and lateral acceleration of each car body are limited within a given safety interval during lane change. To sum up, the control algorithm can better follow the reference path on the low adhesion road and has good stability.

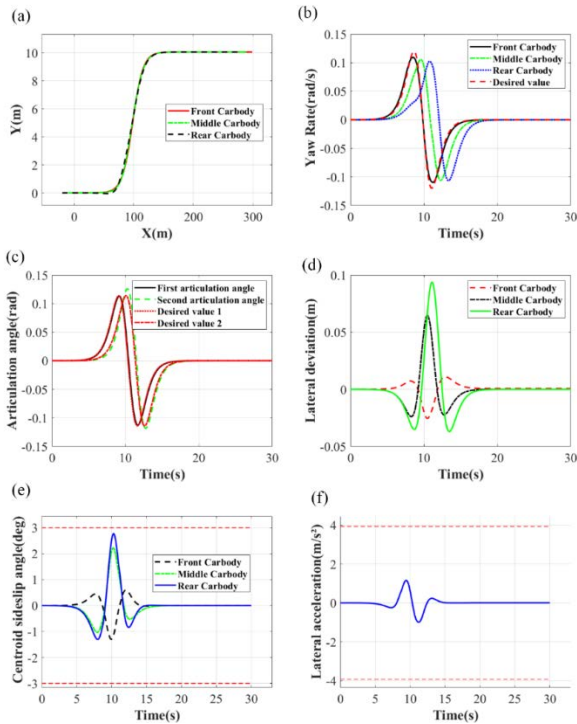


Fig. 10. Trajectory tracking control effect on the low adhesion road.

**Analysis of Control Effect under Different Speeds**

To verify the robustness of the controller to the change of the speed, the controller with the same parameters is used to control the VTT following the reference path, and the control effect of the controller under different speeds is analyzed. From low speed to medium high speed, three speeds are selected for the simulation experiment, which are 5m/s, 10m/s and 15m/s, respectively, and select the pavement with better adhesion conditions,  $\mu=0.8$ .

Fig. 11 shows the simulation results. Fig. 11(a) shows that at different speeds, the maximum lateral deviation of train body centroid at different speeds are 0.029m, 0.053m and 0.082m respectively, which are kept in a small range, indicating that the train has good path following performance and strong robustness to speed. Fig. 11(b) and Fig. 11(c) show that the centroid sideslip angle and lateral acceleration of the rear body of the train always remain within the constraint range at different speeds, and are far lower than the limit value, indicating that the train has strong stability. Therefore, the control algorithm can meet the requirements of low speed to medium high speed.

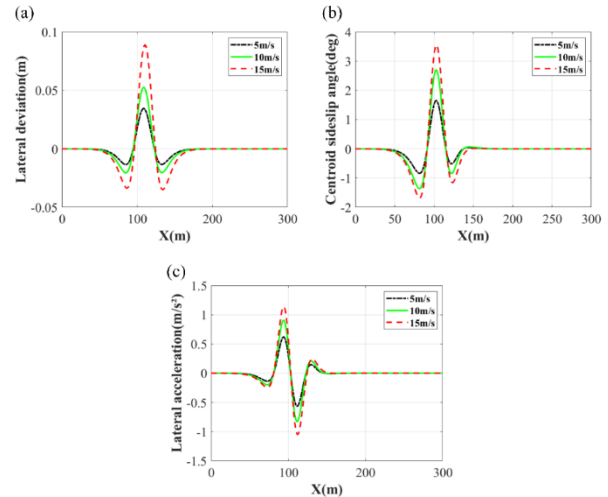


Fig. 11. Control effect comparison at different speeds.

**Analysis of Control Effect under Combined Curve Condition**

In the actual operation, the train will run on various combined lines, and the change of line curvature is also an external interference. Therefore, it is necessary to analyze the adaptability of the control algorithm to the combined curve. Fig. 12 shows the designed simulation test curve, mainly including straight line, large curvature radius curve, small curvature radius curve, positive and negative curvature radius change. Table 2 shows the specific parameters, with the minimum curvature radius of 25m and the maximum curvature radius of 50m.

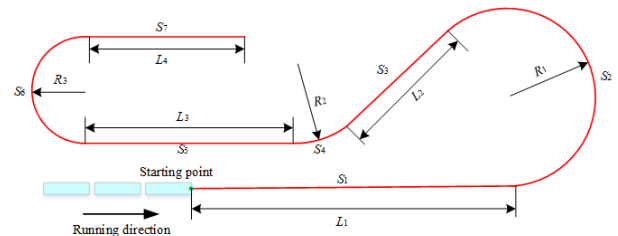


Fig. 12. Combined test curve.

Table 2. Reference line parameters.

| Name | Type           | Size parameters | Speed |
|------|----------------|-----------------|-------|
| S1   | Straight line  | L1 =200m        | 10m/s |
| S2   | Circular curve | R1 =50m         |       |
| S3   | Straight line  | L2 =70m         |       |
| S4   | Circular curve | R2 =50m         |       |
| S5   | Straight line  | L3 =170m        |       |
| S6   | Circular curve | R3 =25m         |       |
| S7   | Straight line  | L4 =100m        |       |

Fig. 13 is the control effect under combined curve. It can be seen from Fig. 13(a) that VTT can well

follow the combined curve, and from the enlarged diagram of the intersection of each straight line and curve, it can be seen that the train can well adapt to the change of curve and has good adaptability. Fig. 13(b) shows the lateral deviation of the train. At the intersection of straight line/curve, the lateral deviation of the train changes greatly. From the whole process, the maximum lateral deviation is only 0.018m, which also shows that the train has good path-following performance. Fig. 13(c) shows the change of articulation angle between train bodies. It can be seen that each articulation angle can stably and accurately track the desired value during the operation of the train, ensuring the stability of the train.

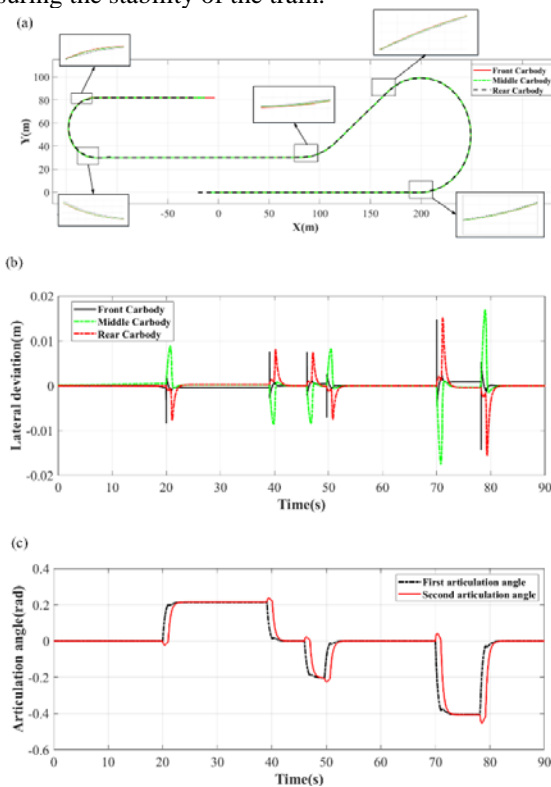


Fig. 13. Control effect under combined curve.

In terms of stability, Fig. 14(a) shows that the centroid sideslip angle of the train has changed greatly at the intersection of straight line and curve, with the maximum value of  $2.96^\circ$ , which is far lower than the limit value. Similarly, Fig. 14(b) shows the lateral acceleration of the train, with the maximum value of  $2.1\text{m/s}^2$ , which is still far lower than the limit value, indicating that the train has strong stability in the process of following the combined curve.

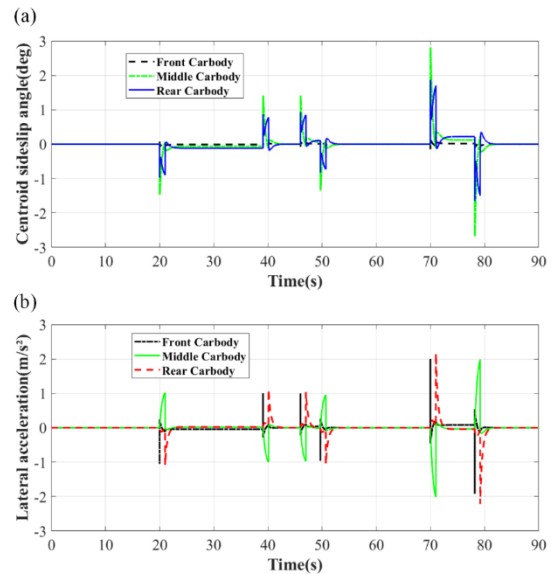


Fig. 14. Dynamic performance index under combined curve.

### CONCLUSIONS

In this paper, the optimal preview control method of multi-objective comprehensive dynamics for virtual track train path following has been proposed. By constructing the reference value sequence including the path following performance index and yaw stability index, and introducing the prediction information, the track following performance and stability requirements of the virtual track train can be considered, and the reaction speed of the control system can be improved. Through simulation test analysis, the following conclusions can be drawn:

(1) The simulation results show that the proposed algorithm can improve the response speed of train following and adapt to the curve path better than that without comprehensive preview information. The maximum lateral deviation is  $0.053\text{m}$ , which is reduced by 89% and greatly improves the accuracy of train following. At the same time, the centroid sideslip angle and lateral acceleration of the train are kept within the set safety range, indicating that the train has good stability.

(2) Through simulation analysis, the control algorithm can meet the adaptability requirements of the train under the condition of low adhesion road. When the train follows the lane changing path on the lane changing path with the adhesion coefficient 0.4, the maximum lateral deviation is  $0.09\text{m}$ , the maximum the centroid sideslip angle is  $2.81^\circ$ , which is within the safety range of  $\pm 3^\circ$ , and the maximum lateral acceleration is  $1.03\text{m/s}^2$ , all of which are within the safe range.

(3) The control algorithm can adapt to the change of train speed from low speed to medium high speed. When the train runs at a low speed of  $5\text{m/s}$ , the maximum lateral deviation of the car body is  $0.31\text{m}$ . When the train runs at higher speed of  $15\text{m/s}$ , the

maximum lateral deviation of the car body is 0.89m, and the dynamic performance index of the train at different speeds remains within the safe range.

(4) The control algorithm can adapt to the sudden change of the composite curve curvature. The maximum lateral deviation of the train at the intersection of the minimum curve with a radius of 25m and the straight line is 0.018m. and the dynamic performance index of the train on the composite curve curvature remains within the safe range.

### ACKNOWLEDGMENT

This work was supported by Science and Technology Research and Development Plan of China Railway Corporation (2017G003-A).

### REFERENCES

Astolfi, A., Bolzern, P., Locatelli, A., "Path-Tracking of a Tractor-Trailer Vehicle Along Rectilinear and Circular Paths:A Lyapunov-Based Approach," *IEEE Trans Robot Autom*, Vol 20, No.1, pp.154-160(2004).

Boucheret, J.M., "Briefing: The CIVIS optically-guided urban transport system," *Proc Inst Civil Eng-Munic Eng*, Vol 157, No.1, pp.13-15(2004).

Bolzern, P., DeSantis, R.M., Locatelli, A., "An Input-Output Linearization Approach to the Control of an n-Body Articulated Vehicle," *J Dyn Syst Meas Control-Trans ASME*, Vol 123, No. 3, pp.309-316(2001).

Georges, B., "Analysis of the discomfort feeling of standing bus passengers on the TEOR-T1 Rouen bus lane," *Transport Research Arena-Europe 2012*, Vol 48, Athens, Greece, pp. 425-434(2012).

Feng, J., Xiao, L., Hu, YQ., "Intelligent rail express system," *Control and Information Technology*, Vol 2020, No.1, pp.1-12(2020).

Han, P., Zhang, WH., "The designation of a new kind of green streetcar based on virtual tracks and key technologies," *Appl Mech Mater*, Vol 714, No.2015, pp.80-84(2015).

Murphy, R.R., "Human-robot interaction in rescue robotics," *IEEE T Syst Man Cy C*, Vol 34, No.2, pp.138-153(2004).

Sampei, M., Tamura, T., Kobayashi, T., et al., "Arbitrary Path Tracking Control of Articulated Vehicles Using Nonlinear Control Theory," *IEEE Trans Control Syst Technol*, Vol 3, No.1, pp.125-131(1995).

Van Zanten, A.T., Erhardt, R., Landesfeind, K., et al., "VDC Systems Development and Perspective," *SAE Transactions*, Vol 107, No.6, pp.424-444(1998).

Wagner, S., Nitzsche, G., Huber, R., "Advanced

Automatic Steering Systems for Multiple Articulated Road Vehicles," *Proceedings of the ASME 2013 International Mechanical Engineering Congress and Exposition*, Vol 13, San Diego, USA, pp.1-11(2013).

Yuan, X.W., Feng, J.H., Hu, Y.Q., et al., "Intelligent tram automatic tracking perception and control system," *Control inf technol*, Vol 2020, No. 1, pp.19-26(2020).

Yamaguchi, H., Kameyama, R., Kawakami, A., "A Path-Following Feedback Control Law of a Five-Axle, Three-Steering Coupled-Vehicle System," *J Robot Mechatron*, Vol 26 No.5, pp.551-565(2014).

### APPENDIX

$$\begin{aligned}
 p_{11} &= v_x(m_1 + m_2 + m_3); \\
 p_{12} &= -[m_2(L_1 + L_2) + m_3(L_1 + L_2 + L_{2r} + L_3)]; \\
 p_{13} &= m_2L_2 + m_3(L_3 + L_2 + L_{2r}); \\
 p_{14} &= \frac{[k_{2f}(L_2 - a_2) + k_{2r}(L_2 + b_2) + k_{3f}(L_2 + L_{2r} + L_3 - a_3) + k_{3r}(L_2 + L_{2r} + L_3 + b_3)]}{v_x}; \\
 p_{15} &= m_3L_3; \quad p_{16} = \frac{[k_{3f}(L_3 - a_3) + k_{3r}(L_3 + b_3)]}{v_x}; \\
 p_{21} &= -v_xL_1(m_2 + m_3); \\
 p_{22} &= L_{21} + m_2L_1(L_1 + L_2) + m_3L_1(L_1 + L_2 + L_{2r} + L_3); \\
 p_{23} &= -[m_2L_1L_2 + m_3L_1(L_2 + L_{2r} + L_3)]; \\
 p_{24} &= -\frac{[k_{3f}L_1(L_2 + L_{2r} + L_3 - a_3) + k_{3r}L_1(L_2 + L_{2r} + L_3 + b_3) + k_{2r}L_1(L_2 + b_2)]}{v_x}; \\
 p_{25} &= -m_3L_1L_3; \quad p_{26} = \frac{[k_{3f}L_1(L_3 - a_3) + k_{3r}L_1(L_3 + b_3)]}{v_x}; \\
 p_{31} &= -[m_2L_2 + m_3(L_2 + L_{2r})]; \\
 p_{32} &= L_{22} + m_2L_2(L_1 + L_2) + m_3(L_2 + L_{2r})(L_1 + L_2 + L_{2r} + L_3); \\
 p_{33} &= -[L_{22} + m_2 * L_2^2 + m_3(L_2 + L_{2r})(L_2 + L_{2r} + L_3)]; \\
 p_{34} &= -\frac{[k_{2f}c_{2f}(L_2 - a_2) + k_{2r}(L_2 + b_2)^2 + (L_2 + L_{2r})\{k_{3f}(L_2 + L_{2r} + L_3 - a_3) + k_{3r}(L_2 + L_{2r} + L_3 + b_3)\}]}{v_x}; \\
 p_{35} &= -m_3L_3(L_2 + L_{2r}); \quad p_{36} = -\frac{(L_2 + L_{2r})[k_{3f}(L_3 - a_3) + k_{3r}(L_3 + b_3)]}{v_x}; \\
 p_{41} &= -m_3L_3v_x; \quad p_{42} = L_{23} + m_3L_3(L_1 + L_2 + L_{2r} + L_3); \\
 p_{43} &= -[L_{23} + m_3L_3(L_2 + L_{2r} + L_3)]; \\
 p_{44} &= -\frac{[k_{3f}c_3(L_2 + L_{2r} + L_3 - a_3) + k_{3r}(L_3 + b_3)(L_2 + L_{2r} + L_3 + b_3)]}{v_x}; \\
 p_{45} &= -(L_{23} + m_3L_3^2); \quad p_{46} = -\frac{[k_{3f}c_3(L_3 - a_3) + k_{3r}(L_3 + b_3)^2]}{v_x}; \\
 q_{11} &= -(k_{1f} + k_{1r} + k_{2f} + k_{2r} + k_{3f} + k_{3r}); \\
 q_{12} &= -(m_1 + m_2 + m_3)v_x + [k_{1r}b_3 - k_{1f}a_1 + k_{2f} * (L_1 + L_2 - a_2) + k_{2r}(L_1 + L_2 + b_2) + k_{3f}(L_1 + L_2 + L_{2r} + L_3 - a_3) + k_{3r}(L_1 + L_2 + L_{2r} + L_3 + b_3)]/v_x; \\
 q_{14} &= -(k_{2f} + k_{2r} + k_{3f} + k_{3r}); \\
 q_{21} &= k_{1r}b_1 - k_{1f}a_1 + (k_{2f} + k_{2r} + k_{3f} + k_{3r})L_1; \\
 q_{22} &= v_xL_1(m_2 + m_3) - [k_{1f}a_1^2 + k_{1r}b_1^2 + k_{2f}L_1(L_1 + L_2 - a_2) + L_{2r}L_1(L_1 + L_2 + b_2) + k_{3f}L_1(L_2 + L_{2r} + L_3 - a_3) + k_{3r}L_1(L_1 + L_2 + L_{2r} + L_3 + b_3)]/v_x; \\
 q_{24} &= L_1(k_{2f} + k_{2r} + k_{3f} + k_{3r}); \quad q_{26} = L_1(k_{3f} + k_{3r}); \\
 q_{31} &= k_{2f}c_{2f} + k_{2r}(L_2 + b_2) + (L_2 + L_{2r})(k_{3f} + k_{3r}); \\
 q_{32} &= v_x[m_2L_2 + m_3(L_2 + L_{2r})] - [k_{2f}c_{2f}(L_1 + L_2 - a_2) + k_{2r}(L_2 + b_2)(L_1 + L_2 + b_2) + k_{3f}(L_2 + L_{2r})(L_2 + L_{2r} + L_3 - a_3) + k_{3r}(L_2 + L_{2r})(L_1 + L_2 + L_{2r} + L_3 + b_3)]/v_x; \\
 q_{34} &= k_{2f}c_{2f} + k_{2r}(L_2 + b_2) + (k_{3f} + k_{3r})(L_2 + L_{2r}); \\
 q_{36} &= (k_{3f} + k_{3r})(L_2 + L_{2r}); \\
 q_{41} &= k_{3f}c_3 + k_{3r}(L_3 + b_3); \\
 q_{42} &= m_3L_3v_x - [k_{3f}c_3(L_2 + L_{2r} + L_3 - a_3) + k_{3r}(L_3 + b_3)L_1 + L_2 + L_{2r} + L_3 + b_3)]/v_x; \\
 q_{44} &= k_{3f}c_3 + k_{3r}(L_3 + b_3); \quad q_{46} = k_{3f}c_3 + k_{3r}(L_3 + b_3); \\
 r_{11} &= r_{12} = k_{1f}; \quad r_{13} = r_{14} = k_{1r}; \quad r_{15} = r_{16} = k_{2f}; \quad r_{17} = r_{18} = k_{2r}; \\
 r_{19} &= r_{110} = k_{3f}; \quad r_{111} = r_{112} = k_{3r}
 \end{aligned}$$

$$\begin{aligned}
r_{21} = r_{22} = k_{1f}a_1; r_{23} = r_{24} = -L_1k_{1r}; r_{25} = r_{26} = -L_1k_{2f}; \\
r_{27} = r_{28} = -L_1k_{2r}; r_{29} = r_{210} = -L_1k_{3f}; \\
r_{211} = r_{212} = -L_1k_{3r}; r_{213} = r_{215} = d; r_{214} = r_{216} = -d; \\
r_{31} = r_{32} = -c_{2f}k_{2f}; r_{33} = r_{34} = -(L_2 + b_2)k_{2r} \\
r_{35} = r_{36} = -(L_2 + b_2)k_{3f}; r_{37} = r_{38} = -(L_2 + b_2)k_{3r}; r_{39} = \\
r_{311} = d; r_{310} = r_{312} = -d; \\
r_{41} = r_{42} = -c_3k_{3f}; r_{43} = r_{44} = -c_3(L_3 + b_3); r_{45} = r_{47} = d; \\
r_{46} = r_{48} = -d; \\
a_{31} = a_{32} = a_1; a_{33} = a_{34} = -L_1; a_{35} = a_{36} = -L_1; a_{37} = \\
a_{38} = -L_1; a_{39} = a_{310} = -L_1; \\
a_{311} = a_{312} = -L_1; a_{313} = a_{315} = d; a_{314} = a_{316} = -d; a_{31} = \\
a_{32} = -c_{2f}; a_{33} = a_{34} = -(L_2 + b_2) \\
a_{35} = a_{36} = -(L_2 + b_2); a_{37} = a_{38} = -(L_2 + b_2); a_{39} = \\
a_{311} = d; a_{310} = a_{312} = -d; \\
a_{41} = a_{42} = -c_3; a_{43} = a_{44} = -c_3(L_3 + b_3); a_{45} = r_{47} = d; \\
r_{46} = r_{48} = -d \\
L_1 = b_1 + c_1; L_2 = a_2 + c_{2f}; L_{2r} = b_2 + c_{2r}; L_3 = a_3 + c_3
\end{aligned}$$

## NOMENCLATURE

- $m_1$  Front car body mass  
 $m_2$  Middle car body mass  
 $m_3$  Rear car body mass  
 $I_{z1}$  Front car body yaw moment of inertia  
 $I_{z2}$  Middle car body yaw moment of inertia  
 $I_{z3}$  Rear car body yaw moment of inertia  
 $a_1$  Distance between the front axle of the front vehicle and the mass center of the car body  
 $b_1$  Distance between the rear axle of the front vehicle and the mass center of the car body  
 $c_1$  Distance from the rear axle of the front vehicle to the first articulation point  
 $a_2$  Distance between the front axle of the middle vehicle and the mass center of the car body  
 $b_2$  Distance between the rear axle of the middle vehicle and the mass center of the car body  
 $c_2$  Distance from the front axle of the middle vehicle to the first articulation point  
 $c_{2r}$  Distance from the rear axle of the middle vehicle to the second articulation point  
 $a_3$  Distance between the front axle of the rear vehicle and the mass center of the car body  
 $b_3$  Distance between the rear axle of the rear vehicle and the mass center of the car body  
 $c_3$  Distance from the front axle of the rear vehicle to the second articulation point  
 $k_{1f}$  Tire cornering stiffness of front axle of front vehicle  
 $k_{1r}$  Tire cornering stiffness of rear axle of front vehicle  
 $k_{2f}$  Tire cornering stiffness of front axle of middle vehicle  
 $k_{2r}$  Tire cornering stiffness of rear axle of middle vehicle  
 $k_{3f}$  Tire cornering stiffness of front axle of rear vehicle  
 $k_{3r}$  Tire cornering stiffness of rear axle of rear vehicle

# 虛擬軌道列車路徑跟蹤的多目標綜合動力學最優預見控制方法

張讓 沈鋼

同濟大學鐵道與城市軌道交通研究院

## 摘要

本文提出了一種多目標綜合動力學的最優預見控制方法，以提高虛擬軌道列車（VTT）在路徑跟蹤過程中的移動性。首先，建立了VTT的6自由度線性參考動力學模型，以橫向速度、橫擺率、第一鉸接和第二鉸接角為控制變量，根據已知的參考路徑信息導出列車參考狀態變量。然後，基於最優預見控制理論，考慮VTT動力學的約束，設計了一種多目標綜合動態控制算法。最後，為了全面分析該算法的可行性，通過多體動力學軟件和MATLAB/Simulink的聯合仿真，分別驗證了該控制算法對道路附著條件、速度和組合曲線的魯棒性。